МАТЕМАТИКА И МАТЕМАТИЧЕСКО ОБРАЗОВАНИЕ, 2018
MATHEMATICS AND EDUCATION IN MATHEMATICS, 2018
Proceedings of the Forty-seventh Spring Conference
of the Union of Bulgarian Mathematicians
Borovets, April 2–6, 2018

DIGITAL IMAGE PROCESSING WITH APPLICATION IN INDUSTRIAL COMPUTED TOMOGRAPHY*

Stanislav Harizanov

Digital image processing is a vastly emerging and extremely active research field, that combines mathematical and computer science knowledge, and has applications in practically all our daily activities. This paper is devoted to denoising two-dimensional images, corrupted by Poisson noise. Various multi-constrained generalizations of a single-constrained convex optimization model, previously developed by the author and co-authors, are introduced, theoretically motivated, and experimentally compared. As a byproduct, an innovative procedure for localization of the image edges and singularities is demonstrated. It can be used in industrial Computed Tomography for the purposes of non-destructive testing.

1. Introduction. Poisson noise typically occurs in processes of counting particles. This is exactly the case in computed tomography (CT), where the gray-scale pixel intensities of the 2D radiographic images are based on the corresponding X-ray amount, captured by the scanner's flat panel detector. As the name suggests, this type of noise is modeled by Poisson distributed random variable whose mean and variance coincide with the real (noise-free) gray-scale value of the corresponding pixel. Because of the mean/variance relationship of the Poisson distribution, denoising here is a nonlinear and complicated process, which is still actively studied nowadays. This paper is devoted to image denoising, based on constrained convex optimization. In general, penalized optimization is more computationally efficient, but there is no procedure for choosing a suitable penalizer λ. On the other hand, constrained optimization is both mathematically and computationally more complex, but the optimal parameter τ can be statistically estimated a priori.

2. Image denoising via constrained energy minimization.

2.1. Single-constrained denoising model. Let $\bar{\mathbf{u}} \in [0,\nu]^{n_1\times n_2}$ be a noise-free two dimensional gray-scale image of size $n := n_1 n_2$ and maximal intensity ν, while $\mathbf{f} = \mathcal{P}(\bar{\mathbf{u}})$ is the given (observed) noisy realization of it. Here $\mathcal{P}$ denotes an independent Poisson noise corruption process. In this paper we consider the ill-posed inverse problem of recovering $\bar{\mathbf{u}}$ from $\mathbf{f}$ and apply the Total Variation (TV) [6] constrained optimization model

$$\mathbf{u} = \operatorname*{argmin}_{u\in[0,\nu]^n} \|\nabla u\|_{2,1} \quad \text{subject to} \quad \|T(u) - T(\mathbf{f})\|_2^2 \le \tau_A, \tag{1}$$

*2010 Mathematics Subject Classification: 68U10, 46N10, 65D15.
Key words: Image denoising, Gaussian Blur, edge detection, constrained convex optimization.
This research is supported by the Bulgarian National Science Fund under grant No. BNSF-DM02/2.

where $\nabla \in \mathbb{R}^{2n\times n}$ is the discrete gradient operator (forward differences and Neumann boundary conditions are used), the $\ell_{2,1}$ norm $\|\cdot\|_{2,1}$ sums the lengths of the pixel gradients, T is the *Anscombe transform* [5]

$$T\colon [0,+\infty)^n \to (0,+\infty)^n\colon u=(u_i)_{1\le i\le n} \mapsto 2\left(\sqrt{u_i+\frac{3}{8}}\right)_{1\le i\le n},$$

and $\tau_A > 0$ describes the size of the constrained set. The Anscombe transform is a variance-stabilizing transformation (VST) which transforms Poisson noise into a Gaussian one with zero mean and unit variance. Hence, in the transformed domain we lack the mean-variance relation of the Poisson distribution and the intensity of the noise is independent on the intensity of the pixel. Furthermore, for large-size images the sampled variance $\|T(\bar{\mathbf{u}})-T(\mathbf{f})\|_2^2/n$ closely approximates the theoretical variance 1, meaning that $\tau_A = n$ is the most appropriate statistical choice. In this case, the constrained set is an n-dimensional ball in the transformed domain with radius $\sqrt{n}$, centered at $T(\mathbf{f})$. The true image $\bar{\mathbf{u}}$ lies on the boundary (the n-dimensional sphere) with high probability.

The idea behind this class of mathematical models is relatively simple. One chooses a convex energy functional, estimates an admissible set that contains the true image $\bar{\mathbf{u}}$, and then – finds the element with the smallest energy in it, hoping this to be $\bar{\mathbf{u}}$ itself. By definition noise is a random variation of the image gray-scale intensity, thus noisy images possess higher energy. The admissibility of $\bar{\mathbf{u}}$ guarantees that the minimizer has smaller energy than $\bar{\mathbf{u}}$, which implies good denoising quality of such an approach. On the other hand, apart from the noise component, the image edges and singularities that capture most of the structural information and are the essential substance of $\bar{\mathbf{u}}$ also increase the energy level. Therefore, together with the noise removal, we lose contrast on the edges and oversmooth the output. As a result some image details can be completely lost. The larger the admissible set the bigger the oversmoothing effect.

The TV norm is more robust towards Gaussian noise than the classical ℓ_2 norm and leads to sparser gradient $\nabla\mathbf{u}$ for the minimizer. As long as the constrained set is nonempty and does not contain constant images, the problem (1) admits a unique solution, which lies on the constraint boundary, meaning that our admissible set is the n-dimensional sphere. The minimizer can be computed by a **p**rimal-**d**ual **h**ybrid **g**radient algorithm [7, 8] with an extrapolation (**m**odification) of the dual variable (PDHGMp). At each iteration step, we compute n epigraphical projections [9] with respect to a 1D convex function related to T [1]. The algorithms' description can be found in [1, Section 4], while its parallel implementation is the object of [4].

2.2. Multi-constrained modifications of the model. The admissible set for (1) is too large and the TV norm of the minimizer $\mathbf{u}$ could be several times smaller than the TV norm of the noise-free image $\bar{\mathbf{u}}$, as observed in [2]. Hence, we want to restrict the former without losing $\bar{\mathbf{u}}$ as a member. In [2] we consider domain decomposition techniques for achieving that, namely we solve the multi-constrained optimization problem

$$\mathbf{u} = \operatorname*{argmin}_{u\in[0,\nu]^n} \|\nabla u\|_{2,1} \quad \text{subject to} \quad \|T(u)-T(\mathbf{f})\|_{A_i} \le \tau_i, \quad i=1,\dots,K, \tag{2}$$

where $\{A_i\}_{i=1}^K$ is a non-overlapping tessellation of the image domain, and $\|\cdot\|_{A_i}$ is a short notation for the squared ℓ_2-norm, restricted to the region A_i. In this approach, the n-dimensional sphere is replaced by a direct product of lower dimensional ones. Those

admissible sets are subsets of the original one, thus the energy of the minimizer in (2) is higher than the energy of the minimizer in (1), leading to outputs with better quality. The bottleneck here is related to the admissibility of $\bar{\mathbf{u}}$ and the solvability of the multi-constrained optimization problem. The size of A_i should be big enough, so that the sampled variance still approximates well the true one on the region and the statistical arguments for the choice of τ_i remain valid. Furthermore, each region should contain image edges, otherwise constant solutions may appear for some of the patches and the minimizer will no longer belong to the boundary of the constrained set. On the other hand, the overall quality improvement of the solution is relatively small, meaning that the benefits from the domain decomposition are quite limited.

In [3] we develop a different machinery for attacking the problem. Assuming that we have two independent noisy observations $\mathbf{f}^1$ and $\mathbf{f}^2$ of $\bar{\mathbf{u}}$ with identical noise characteristics, than we can study the following model problem

$$\mathbf{u} = \underset{u\in[0,\nu]^n}{\operatorname{argmin}} \|\nabla u|\|_{2,1} \text{ subject to } \begin{cases} \left\|T(u) - T(\mathbf{f}^1)\right\|_2^2 \leq \dfrac{1}{2}\left\|T(\mathbf{f}^2) - T(\mathbf{f}^1)\right\|_2^2 \\ \\ \left\|T(u) - T(\mathbf{f}^2)\right\|_2^2 \leq \dfrac{1}{2}\left\|T(\mathbf{f}^2) - T(\mathbf{f}^1)\right\|_2^2. \end{cases} \tag{3}$$

Here, we use that $\mathbf{f}^1$ and $\mathbf{f}^2$ are uncorrelated and apply n-dimensional Pythagorean theorem

$$\left\|T(\bar{\mathbf{u}}) - T(\mathbf{f}^1)\right\|_2^2 + \left\|T(\bar{\mathbf{u}}) - T(\mathbf{f}^2)\right\|_2^2 = \left\|T(\mathbf{f}^2) - T(\mathbf{f}^1)\right\|_2^2.$$

The benefits of such model are several. First, it is not restricted only to Poisson noise and we do not even need to know the exact noise characteristics a priori, as long as they are identical for both input images. Second, the parameter τ_A is explicitly derived and the true image $\bar{\mathbf{u}}$ belongs to the border of the constrained set with high probability, which increases with the size of $\bar{\mathbf{u}}$. Third, the admissible set is an intersection of two n-dimensional spheres in the transformed domain, and thus is an $n-1$ dimensional sphere so we have reduced its dimensionality. On the other hand, the assumptions on $\mathbf{f}^1$ and $\mathbf{f}^2$ are naturally fulfilled in practice. Indeed, the noise characteristics of an image typically depend on the parameters of the acquisition device, so when $\mathbf{f}^1$ and $\mathbf{f}^2$ are generated in a small time interval by the same device under the same conditions their noise components have identical probability distribution and are uncorrelated. We have experimentally confirmed this on several Computed Tomography (CT) scanners.

Equation (3) can be straightforwardly generalized for arbitrary many observations $\{\mathbf{f}^i\}$ and the PDHGMp solver for (1) can be easily adapted to the multi-frame setting. However, the conducted numerical experiments in [3] indicate that we gain the highest image quality within the transition from one to two observations. Furthermore, in case more than two observations have different candidates for τ_A, it is unclear which one of them is optimal, thus we cannot guarantee admissibility of $\bar{\mathbf{u}}$. The latter is a serious obstacle as the constrained set might be empty and the problem – ill-posed.

2.3. Introducing phantom blur. The original single-constrained model proposed in [1] is not only for denoising but also for deblurring purposes, i.e., when $\mathbf{f} = \mathcal{P}(H\bar{\mathbf{u}})$, where $H \in [0,\nu]^{n\times n}$ is a blur operator, corresponding to a convolution with a Gaussian kernel. In more detail, in 1D we fix a positive constant σ, sample the function $e^{-x^2/2\sigma^2}/(\sigma\sqrt{2\pi})$ at the integer points in the interval $[-3\sigma, 3\sigma]$, and then normalize the

set to sum up to one. We call the corresponding values $\{\omega_i\}_{-\lfloor 3\sigma\rfloor}^{\lfloor 3\sigma\rfloor}$ *blur weights* and given a signal vector v we construct its blur version via

$$(Hv)_i = \sum_{j=-\lfloor 3\sigma\rfloor}^{\lfloor 3\sigma\rfloor} w_j v_{i+j}.$$

In 2D, we consider tensor products. For example, the blur weights for $\sigma = 0.5$ are documented in Table 1. We see that the brightness of every pixel in $H\bar{\mathbf{u}}$ is a weighted average of the brightnesses of its neighbors within a 5×5 stencil.

Table 1. 2D blur weights for $\sigma = 0.5$

0.000002	0.000212	0.000922	0.000212	0.000002
0.000212	0.024745	0.107391	0.024745	0.000212
0.000922	0.107391	0.466066	0.107391	0.000922
0.000212	0.024745	0.107391	0.024745	0.000212
0.000002	0.000212	0.000922	0.000212	0.000002

Blur operators are often used for denoising as they smoothen the data. Due to the normalization of the blur weights they preserve the overall image brightness (the sum of the intensities of all pixels) and constant regions. Meanwhile, they decrease the contrast of the image edges. Comparing with the properties of the minimizer $\mathbf{u}$ for (1), we find huge resemblance. Blurred images possess lower energy than their counterparts, therefore it makes sense to assume that $\mathbf{u} \approx H\bar{\mathbf{u}}$ rather than $\mathbf{u} \approx \bar{\mathbf{u}}$. The current subsection is devoted to this approach. We consider

$$\mathbf{u} = \operatorname*{argmin}_{u\in[0,\nu]^n} \|\nabla u\|_{2,1} \quad \text{subject to} \quad \|T(Hu) - T(\mathbf{f})\|_2^2 \le \tau_A, \tag{4}$$

where H is suitably chosen. Experimentally, $\sigma = 0.5$ seems to be optimal with respect to the quality of the output. We run all our numerical experiments in the next section for this blur operator. There are additional theoretical arguments why this choice of σ is meaningful. The original pixel gray-scale intensity contributes approximately the same as all its neighboring pixels combined to the formation of the corresponding blurry pixel gray-scale intensity (see Table 1). Therefore, such blur operator preserves local extrema and if the i-th pixel has maximal/minimal brightness within the original 5×5 frame around it, then it has maximal/minimal brightness within the blurred 5×5 frame, as well. Consequently, no inversions around the image edges can appear during the blurring. When σ increases – this property is lost, while when σ decreases – the blurring effect also decreases.

The question about the admissibility of $\bar{\mathbf{u}}$ for (4) is equivalent to checking if $\|T(H\bar{\mathbf{u}}) - T(\mathbf{f})\|_2^2 = \|T(\bar{\mathbf{u}}) - T(\mathbf{f})\|_2^2$. Since $\sum_i (H\bar{\mathbf{u}})_i = \sum_i \bar{\mathbf{u}}_i$ and applying the mean value theorem we estimate

$$\|T(H\bar{\mathbf{u}}) - T(\mathbf{f})\|_2^2 - \|T(\bar{\mathbf{u}}) - T(\mathbf{f})\|_2^2$$

$$= 4\sum_i \left((H\bar{\mathbf{u}})_i + \mathbf{f}_i + \frac{3}{4} \right) + 8\sum_i \sqrt{\mathbf{f}_i + \frac{3}{8}} \left(\sqrt{\bar{\mathbf{u}}_i + \frac{3}{8}} - \sqrt{(H\bar{\mathbf{u}})_i + \frac{3}{8}} \right)$$

$$-4\sum_i \left(\bar{\mathbf{u}}_i + \mathbf{f}_i + \frac{3}{4}\right)$$

$$= 4\sum_i \frac{\sqrt{\mathbf{f}_i + 3/8}}{\sqrt{\xi_i + 3/8}} \left(\bar{\mathbf{u}}_i - (H\bar{\mathbf{u}})_i\right).$$

The intermediate value ξ_i is between $\bar{\mathbf{u}}_i$ and $(H\bar{\mathbf{u}})_i$. When $\sigma = 0.5$ we have

$$0.466066\bar{\mathbf{u}}_i \leq (H\bar{\mathbf{u}})_i \leq \bar{\mathbf{u}}_i + 0.533934 \max_{j \in Frame(i)} (\bar{\mathbf{u}}_j - \bar{\mathbf{u}}_i),$$

meaning that $\dfrac{\sqrt{\mathbf{f}_i + 3/8}}{\sqrt{\xi_i + 3/8}} = \mathrm{O}(1)$, because $\mathbf{f}_i = \mathcal{P}(\bar{\mathbf{u}}_i)$. Without this scaling factor, the sum is zero. Hence, we can indeed assume that $(H\bar{\mathbf{u}})$ also lies on the n-th dimensional sphere that bounds the constrained set.

We can apply all multi-scale approaches from Section 2.2 to (4) instead of (1) and investigate how the introduction of a phantom blur affects the quality of the image reconstruction. This will be done in Section 3.

2.4. Edge detection via image differencing. As already mentioned, constrained energy minimization techniques lead to practically noise-free, but oversmoothed images. The level of oversmoothing depends on the size of the constrained set and the admissibility of the true image $\bar{\mathbf{u}}$. This affects the contrast of the image edges and not the brightness of regular regions. Therefore, we can try localizing the image edges via looking in the difference image $|\mathbf{u}^2 - \mathbf{u}_1|$ of minimizers with respect to different constrained sets. Pixels with high gray-scale intensity should belong to image edges or singularities. We will see in the next section that when $\mathbf{u}^2$ is the "blurred" counterpart of $\mathbf{u}^1$ their difference image provides good visualization for the high-contrast image edges and can serve as a simplified sketch of the original image (the one that we will draw if we are given only pen and paper).

3. Numerical experiments. We conduct two series of numerical experiments. The first one is on synthetic data - standard test images, that are artificially polluted with pure Poisson noise. For this purpose, we apply the MatLab function

`1e12*imnoise(u*1e-12,'poisson').`

Since the original images $\bar{\mathbf{u}}$ are known, we can measure the quality of the different approaches via the functionals peak signal to noise ratio (PSNR) and mean absolute error (MAE), defined as

$$\mathrm{PSNR} = 10\log_{10} \frac{|\max \bar{\mathbf{u}} - \min \bar{\mathbf{u}}|^2}{\frac{1}{n}\|\mathbf{u} - \bar{\mathbf{u}}\|_2^2}, \qquad \mathrm{MAE} = \frac{1}{n\nu}\|\bar{\mathbf{u}} - \mathbf{u}\|_1.$$

All test images are 8-bit ($\nu = 255$) and of medium size (less or equal to 512×512). For each of them we generate two different noisy realizations $\mathbf{f}^1$ and $\mathbf{f}^2$. We denote by $\mathbf{u}^1$ and $\mathbf{u}^2$ their corresponding minimizers of the single-constrained model (1). Images $\{\mathbf{u}^i\}_3^5$ are related to the multi-constrained model (2) applied to $\mathbf{f}^1$. For $\mathbf{u}^3$ we geometrically split the image domain into four identical quadrants and use them as $\{A_i\}_1^4$. For $\mathbf{u}^4$ we split the intensity domain of $\mathbf{u}^1$ and consider only two regions $B_1 := \{i \,|\, \mathbf{u}_i^1 \leq 128\}$ and $B_2 := \{i \,|\, \mathbf{u}_i^1 > 128\}$. For $\mathbf{u}^5$ we use both previous tessellations – the four quadrants and a slightly modified $B_1' := \{i \,|\, \mathbf{u}_i^1 \leq 115\}$ and $B_2' := \{i \,|\, \mathbf{u}_i^1 > 140\}$, together with a buffer region $B_3' := \{i \,|\, 115 < \mathbf{u}_i^1 < 140\}$. The last image $\mathbf{u}^6$ is the solution of (3). For

each $\mathbf{u}^i$ we have also computed its blurred counterpart, where u is replaced by Hu in the definition of the corresponding constrained set.

Table 2. Quantitative comparison of quality of image recovery on synthetic data. Left: without phantom blur. Right: with phantom blur of $\sigma = 0.5$

	Image	cameraman	peppers	Lena	boat
P	$\mathbf{f}^1$	27.122	28.750	25.911	26.995
	$\mathbf{f}^2$	27.102	28.692	25.931	27.002
S	$\mathbf{u}^1$	30.555 / 31.305	34.210 / 35.179	31.609 / 32.358	30.872 / 31.621
	$\mathbf{u}^2$	30.562 / 31.338	34.299 / 35.265	31.580 / 32.331	30.884 / 31.635
N	$\mathbf{u}^3$	30.653 / 31.421	34.188 / 35.165	31.615 / 32.363	30.898 / 31.609
	$\mathbf{u}^4$	30.804 / 31.235	34.596 / 35.498	31.706 / 32.397	31.029 / 31.758
R	$\mathbf{u}^5$	31.029 / 31.495	34.855 / 35.653	31.695 / 32.327	30.726 / 31.177
	$\mathbf{u}^6$	32.599 / 32.437	36.113 / 37.076	33.308 / 33.904	32.634 / 33.139
M	$\mathbf{f}^1$	3.2136	2.7230	3.5481	3.4778
	$\mathbf{f}^2$	3.2209	2.7353	3.5394	3.4779
A	$\mathbf{u}^1$	1.7652 / 1.7153	1.1697 / 1.0752	1.6646 / 1.5564	2.0798 / 1.9479
	$\mathbf{u}^2$	1.7530 / 1.7023	1.1644 / 1.0710	1.6691 / 1.5600	2.0756 / 1.9429
E	$\mathbf{u}^3$	1.7298 / 1.6805	1.1698 / 1.0752	1.6686 / 1.5597	2.0809 / 1.9546
	$\mathbf{u}^4$	1.7299 / 1.7330	1.1507 / 1.0595	1.6495 / 1.5507	2.0449 / 1.9198
$\times 10^{-2}$	$\mathbf{u}^5$	1.6874 / 1.6745	1.1358 / 1.0512	1.6624 / 1.5720	2.1314 / 2.0599
	$\mathbf{u}^6$	1.4357 / 1.4928	0.9616 / 0.8896	1.3982 / 1.3262	1.7345 / 1.6593

The results are summarized in Table 2 and they numerically confirm the theoretical discussion in Section 2. First of all, we observe that the quality of both the noisy data and the single-constrained minimizer is not sensitive towards the particular observation $\mathbf{f}$. For all test images we have similar values in terms of PSNR and MAE for $\mathbf{f}^1$ and $\mathbf{f}^2$, respectively $\mathbf{u}^1$ and $\mathbf{u}^2$. Second, we observe that the potential of the domain decomposition multi-constrained approach is insubstantial. We do not practically gain anything in the case of geometry-based tessellations, while we may gain a little in the case of intensity-based tessellations, as we keep the bright and the dark sides of high-contrast edges in different regions and do not let them merge as easily as in the single-constrained case. The combination of the two may further slightly improve the result ("cameraman" and "peppers") or make it even worse ("Lena" and "boat"). Here, the problem is the cardinality of B_3', which can be too low for the validation of the statistical arguments. The multi-frame approach (3) stably increases the PSNR values by around 2dB and decreases the MAE values by around 3×10^{-3}, compared to the single-frame approach (1). The usage of phantom blur additionally improves the quality of the result. The only exception is the multi-frame setting, applied to "cameraman".

In Fig. 1 we have illustrated the input data and part of the results. We observe that the presence of long, thin details in the input image affects negatively the amount of quality improvement for the output. Indeed, the texture on the boat in "boat" and the camera parts in "cameraman" are fragile towards noise corruption and are badly preserved in the observations $\mathbf{f}$, making their full recovery impossible. On the other hand, when all the objects from the input image are of proper size like in the case of "peppers" the quality improvement for the output is higher. On the last row we

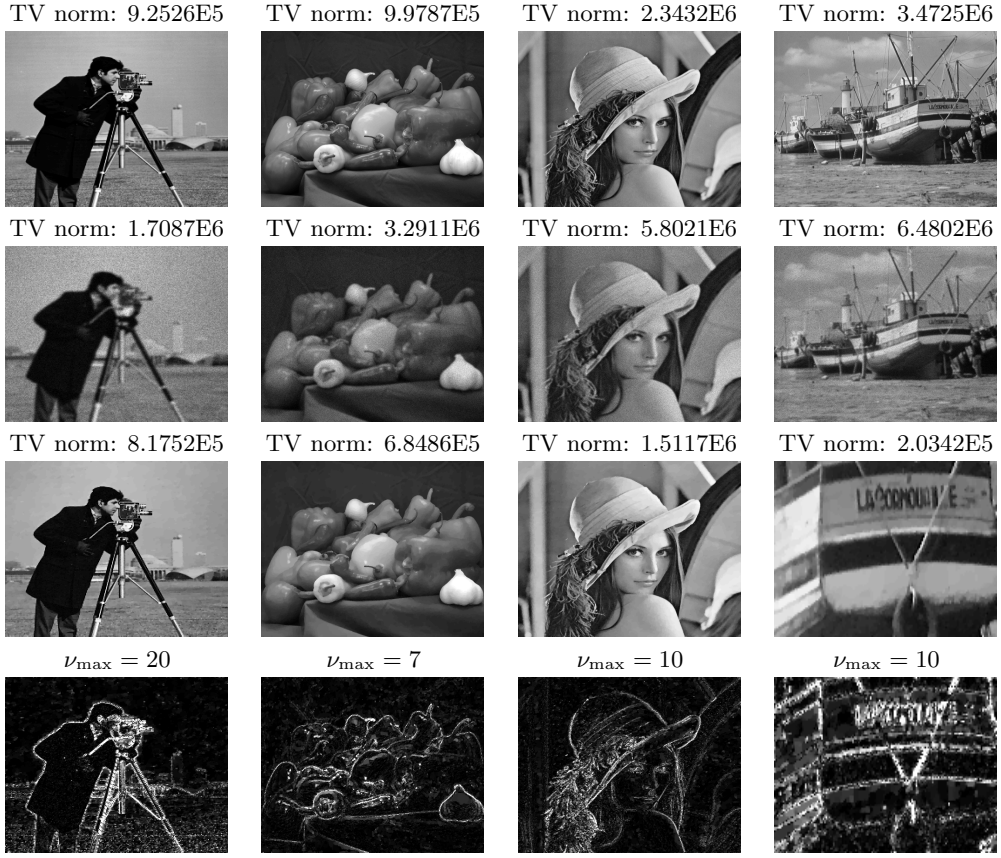

Fig. 1. Denoising and edge detection. From top to bottom: original, noise-free data $\bar{\mathbf{u}}$; observed data $\mathbf{f}$ corrupted by pure Poisson noise; the output image from the blurred version of (3); the difference image between the former and its non-blurred counterpart

have plotted the absolute difference images between the two versions of $\mathbf{u}^6$. For better visualization, we have chosen an intensity level $\nu_{\max}$ and have restricted the image onto the intensity interval $[0, \nu_{\max}]$. In all examples, the image edges are well-localized and no trace of the noise component is present.

The second series of numerical experiments are conducted on real CT data, where the true image and the noise characteristics of the generated images are unknown. Hence, here only the multi-frame approach (3) is applicable, because no a priori information on τ_A is available. Three different image sets have been considered, as illustrated on Fig. 2. All the tests are application-driven. For the first two, we are interested in detecting and analyzing voids in various materials. The presence of voids, their shape and density affect the physical properties of the material. Studying them is a vital part of Material Science. We observe that the difference image between the natural and the blurred versions of (3) can be quite useful for this purpose and the study can be performed without physically damaging the specimen. Furthermore, the two observations $\mathbf{f}^1$ and $\mathbf{f}^2$ are derived from

low-dose and short exposure time scanning processes, making the procedure relatively cheap and suitable for medical CT data, as well. They are 16-bit and of size 1446×1840. The voids cannot be seen with naked eye on the input data, but they are clearly visualized on the difference image. As a third example, we have used scanning data from an ancient coin.

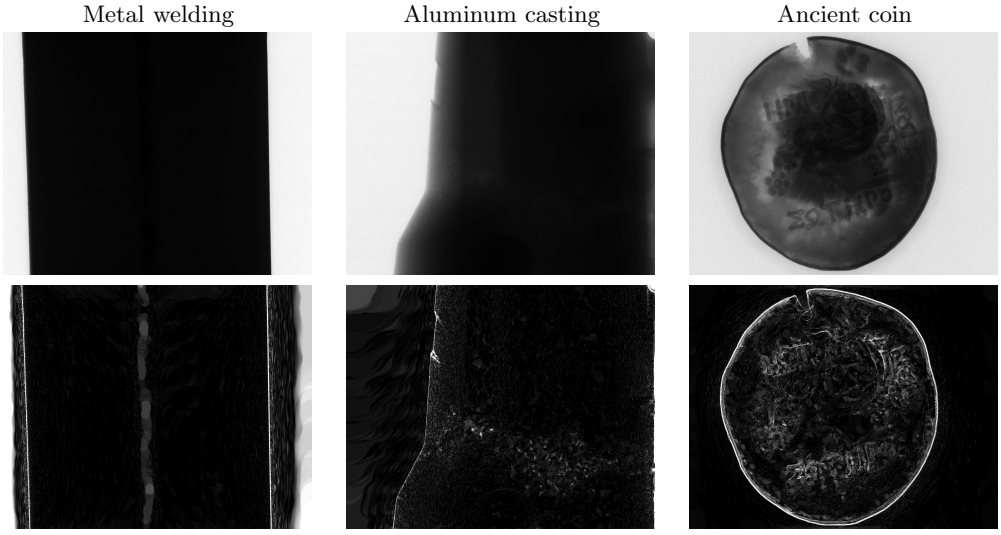

Fig. 2. Edge detection on real industrial data. Left & Center: Non-destructive testing for voids in materials. Right: Application to cultural heritage

4. Concluding remarks. In this paper we introduced and compared several multi-constrained generalizations of the energy minimization model (1), which has application in image denoising. We proposed the usage of a medium phantom blur ($\sigma = 0.5$) in the definition of the constrained sets and numerically investigated its advantages on both synthetic and real data. As a byproduct, the absolute difference image between the corresponding minimizers of the original and the blurred models localizes the image edges and singularities, thus it preserves well the structural information and can be used in industrial Computed Tomography for the purposes of non-destructive testing.

Acknowledgements The author thanks Assoc. Prof. Ivan Georgiev (IICT/IMI–BAS) for providing him with real industrial radiographic data and Assoc. Prof. Ivan Lirkov (IICT–BAS) for running the numerical experiments on them.

REFERENCES

[1] S. Harizanov, J. C. Pesquet, G. Steidl. Epigraphical Projection for Solving Least Squares Anscombe Transformed Constrained Optimization Problems. In: Scale-Space and Variational Methods in Computer Vision (SSVM 2013), LNCS 7893, Berlin, Springer-Verlag, 2013, 125–136.

[2] S. Harizanov. Deblurring Poissonian Images via Multi-constraint Optimization. In: Innovative Approaches and Solutions in Advanced Intelligent Systems, SCI 648, Springer International Publishing Switzerland, 2016, 201–217.
[3] S. Harizanov, I. Lirkov, I. Georgiev. Restoration of Low-dose CT Radiographic Images. In: Short Communications of the International Workshop on Combinatorial Image Analysis (IWCIA'17), Plovdiv, Bulgaria, Rakursy Ltd., 2017, 31–35.
[4] S. Harizanov, I. Lirkov, K. Georgiev, M. Paprzycki, M. Ganzha. Performance analysis of a parallel algorithm for restoring large-scale CT images. *Journal of Computational and Applied Mathematics*, **310** (2017), 104–114.
[5] F. J. Anscombe. The transformation of Poisson, binomial and negative-binomial data. *Biometrika*, **35** (1948), 246–254.
[6] L. I. Rudin, S. Osher, E. Fatemi. Nonlinear total variation based noise removal algorithms. *Physica D*, **60** (1992), 259–268.
[7] A. Chambolle, T. Pock. A first-order primal-dual algorithm for convex problems with applications to imaging. *Journal of Mathematical Imaging and Vision*, **40**, No 1 (2011), 120–145.
[8] T. Pock, A. Chambolle, D. Cremers, H. Bischof. A convex relaxation approach for computing minimal partitions. IEEE Conference on Computer Vision and Pattern Recognition, 2009, 810–817.
[9] G. Chierchia, N. Pustelnik, J.-C. Pesquet, B. Pesquet-Popescu. Epigraphical projection and proximal tools for solving constrained convex optimization problems. *Signal, Image and Video Processing*, **9**, No 8 (2015), 1737–1749.

Stanislav Harizanov
Institute of Information and Communication Technologies
Bulgarian Academy of Sciences
Acad. G. Bontchev Str., Bl. 25A
1113 Sofia, Bulgaria
and
Institute of Mathematics and Informatics
Bulgarian Academy of Sciences
Acad. G. Bontchev Str., Bl. 8
1113 Sofia, Bulgaria
e-mail: sharizanov@parallel.bas.bg

ОБРАБОТКА НА ДИГИТАЛНИ ИЗОБРАЖЕНИЯ С ПРИЛОЖЕНИЕ В ИНДУСТРИАЛНАТА КОМПЮТЪРНА ТОМОГРАФИЯ

Станислав Харизанов

Обработката на дигитални изображения е бързо развиваща се и изключително актуална научна област, съчетаваща знания в сферите на Математиката и Компютърните науки и имаща приложение в почти всички ежедневни дейности. Тази статия е посветена на обезшумяването на двумерни изображения, замърсени с Поасонов шум. В нея се представят и се мотивират теоретично различни обобщения на изпъкналия оптимизационен модел с ограничение, вече разработен от научен екип с участието на автора. Извършен е числен, експериментален сравнителен анализ на различните решения. В допълнение е демонстрирана иновативна процедура за локализиране на ръбовете и особеностите на входното изображение, която би могла да бъде широко използвана в областта на Компютърната томография за нуждите на безразрушителния контрол.